

Explanatory Supplement to the 9P/Tempel 1 IRAS Survey Images

Delivered to University of Maryland

December 29, 2000

Russ Walker

Vanguard Research, Inc.  
5321 Scotts Valley Drive, Suite 204  
Scotts Valley, CA 95066

Revised August 9, 2005  
by PDS-SBN, University of Maryland  
to reflect modifications requested during the PDS Peer Review

## Survey Scan Radiance and Noise Maps - Background

The bulk of the IRAS observation time was spent in the survey mode that systematically mapped the sky with a series of overlapping and confirming scans. This redundancy can be used to produce a survey with fainter limiting magnitude, such as the IRAS Faint Source Survey, or to improve the spatial resolution in the scanned fields. Construction of images from survey data is complicated by the fact that the confirming scans cross each other at varying angles. Construction of comet images also requires compensation for the motion of the comet and the changing spacecraft parallax during the relatively large time interval (>103 minutes) between the confirming scans necessary to build the image. All the images in the delivered set were constructed from survey scans. They are thus "time-averaged" images of the comet emission history. Table 3 at the end of this document lists the Survey Scans used in each "time-averaged" image.

The method for the production of comet images uses a computer algorithm based on the Maximum Correlation Method (MCM) for Image Construction (Aumann, Fowler, and Melnyk, 1990), and closely parallels the "HiRes Processing" performed at IPAC (Melnyk and Rice, 1991). The major departure from the IPAC scheme occurs in the Comet Image Preprocessor (CIPP) where the coordinates of each detector footprint (data sample) are transformed to a moving Sun-referenced coordinate system with the comet at the origin.

The Comet Image Preprocessor (CIPP) - The CIPP program reads the scan data and performs three main functions; 1) transform the coordinates of the data samples to a coordinate system that moves with the comet; 2) remove data artifacts, such as baseline, tails, and radiation hits (glitches) that tend to be magnified by the image construction processing; and 3) associate each data sample with the specific pixels in the map covered by the detector response function and their weights in the observed response. This latter information is stored in an array and is "looked up" by the processor (described below) at each iteration of the image construction.

The Comet Image Processor (CIP) - Once the CIPP has "cleaned up" the scan, the CIP program applies the MCM algorithm to construct high-resolution images of the comet from the survey scans. The spatial response functions of the IRAS detectors that were used are modified versions of those given by Moshir, 1986. They have been "de-tailed" and their response extended to 1% of the peak by approximating the point spread function of the IRAS telescope mirror with a two-dimensional Gaussian blur that contains 85% of the flux from a point source within a circle of diameter 25", 25", 60", and 100" for the 12, 25, 60, and 100 micron bands (Beichman, et al, 1988).

CIP begins with a map of uniform low level radiance, and builds an image by scanning an analytical version of the IRAS focal plane over the map, simulating the IRAS data-taking process. The analytical data samples are compared to the real scan data samples (cleaned by the CIPP) and pixel correction factors determined. Details of this process are given by Aumann, et al, 1990 and Melnyk and Rice, 1991. Building the map is an iterative process, wherein each iteration begins with the most recent estimate of map radiance.

Statistics relating to pixel noise and convergence are generated at each iteration. A typical image will converge after 15 to 40 iterations. For each iteration, two image products were produced from the Tempel 1 survey scans:

A. Radiance Map - The radiance map is the surface brightness image produced by the CIP. Two radiance maps were produced for archive; 1) the map resulting from the first iteration (equivalent to the IPAC FRESCO image, see Melnyk, 1990), and 2) the high-resolution map produced at the final iteration.

B. Photometric Noise Map - This is an image of the internal photometric uncertainty (standard deviation) of the radiance in a pixel as a result of averaging overlapping detector samples. The photometric noise map may be used to estimate the error in aperture photometry of the comet, photometric profiles, and flux ratios.

### **Radiance and Noise Maps - File Designations and Content**

The delivered data set includes radiance and noise images, processing logs, aperture photometry files, the scan list, and a file of the osculating orbital elements used for Tempel 1. IRAS scans are identified by a satellite operations plan (SOP) number. The images are identified by a “mean” SOP number, since several scans are used to make an image. The IRAS observations were made in four spectral bands centered nominally at 12 $\mu$ m, 25 $\mu$ m, 60 $\mu$ m, and 100 $\mu$ m. Radiance images and noise maps are supplied for the first iteration (01) and the final iteration (nn) determined by the convergence of the flux in all the pixels in the scanned path. Thus, the following file names were adopted:

Radiance and Noise Maps in /data/survey/images/:

Radiance Maps (40) – sSOP\_Band\_Iteration#\_radiance.fit  
Noise Maps (40) – sSOP\_Band\_Iteration#\_noise.fit

The numbers in parenthesis above are the number of files that PDS-SBN received. Values for Band are 12 $\mu$ m, 25 $\mu$ m, 60 $\mu$ m, and 100 $\mu$ m. Iteration values are 01 for the first iteration or the number of the final iteration (15 through 40).

For convenience, Russell Walker included the spectral response files of the IRAS detector bands that he used to process the Survey Scans. The 12 $\mu$ m and 100 $\mu$ m files that he used included refinements to the spectral response files available at IPAC. The spectral response files are named /calib/bandN\_WWWum.tab, where N is the IRAS band number, 1, 2, 3, or 4, that is equivalent to WWW, the nominal wavelength (at band center): 12 $\mu$ m, 25 $\mu$ m, 60 $\mu$ m, and 100 $\mu$ m.

The Radiance and Noise Maps are in FITS image format. They have extensive headers that provide all the data that you need to use the images. The following is an example from a 100 $\mu$ m image that converged after 16 iterations.

```

SIMPLE = T / Written by IDL: 27-Dec-2000 17:25:50.00
BITPIX = -32 / IEEE single precision floating point
NAXIS = 2
NAXIS1 = 150 / Fastest varying axis
NAXIS2 = 075 / Slowest varying axis
BSCALE = 1.00000 /
BUNIT = 'Watts/cm2/sr' /
BZERO = 0.000000 /
OBJECT = '9P/TEMPEL 1' / Target
DATAMAX = 3.15750E-10 / Watts/cm2/sr (in-band radiance)
DATAMIN = 0.00000E+00 / Watts/cm2/sr (in-band radiance)
CRVAL1 = 96.94210 / Solar elon of target via orbital elements
CRPIX1 = 77 / X-axis origin, pixel at comet max
CDEL1 = 24 / X-axis pixel width (arcsec)
CTYPE1 = 'ELONGATION' / Angle between IRAS line of sight and Sun
CRVAL2 = 359.40880 / Solar incl of target via orbital elements
CRPIX2 = 37 / Y-axis origin, pixel at comet max
CDEL2 = 24 / Y-axis pixel width (arcsec)
CTYPE2 = 'INCLINATION' / Angle between ecl plane, E-S plane and obs dir
COMMENT COMET Tempel 1 1983 XI
COMMENT FLUX MAP
COMMENT Iteration 016
COMMENT Converged Pixels 09741
COMMENT Jan 2003, PDS Small Bodies Node modified the header:
COMMENT 1) Corrected several keywords and values to standards.
COMMENT 2) Added keyword comments for clarification.
COMMENT 3) Removed peak flux comment line per R.Walker.
COMMENT 4) Added observation-specific keywords at end of header.
COMMENT 5) Image size is 1.0 degree by 0.5 degree.
COMMENT 6) Pixel size is 24 arcsec by 24 arcsec.
FILENAME= 's339_100um_16_radiance.fit' / OUTPUT FILE NAME
COMETMAX= 1.15603E-11 / Watts/cm2/sr (in-band radiance)
WAVE = 100 / Wavelength (microns)
MEAN_JD = 2445529.789 / Mean Julian date of combined observations
MEANDT = '1983-07-14' / Mean UTC date of combined obs
MEANTM = '06:56:09.600' / Mean UTC time of combined obs
MEAN_RA = 205.57081 / deg
MEAN_DEC= -11.23130 / deg
SOP = 339 / Scan Orbit
NOBS = 7 / Number of observations
RHO = 1.492 / Sun-Comet distance (AU)
DELTA = 0.976 / Earth-Comet distance (AU)
PHASE = 42.566 / Phase angle (S-T-O) (deg)
TOBS = 336 / Summed time of observations (sec)
UTCSTART= 2445529.6202 / UTC at start of obs (Julian date)
UTCSTOP = 2445530.0499 / UTC at end of obs (Julian date))
STARTDT = '1983-07-14' / UTC date at start of obs
STARTTM = '02:53:05.360' / UTC time at start of obs
STOPDT = '1983-07-14' / UTC date at end of obs
STOPTM = '13:11:47.180' / UTC time at end of obs
SCSTART = 79843985.36 / IRAS time at start of obs
SCSTOP = 79881107.18 / IRAS time at end of obs
END

```

The image is 150 x 75 pixels (NAXIS1 x NAXIS2).

The coordinate system is solar elongation and inclination, a natural coordinate system for IRAS. Elongation  $\theta$  is the angle between the line of sight and the Sun. Inclination  $I_0$  is the angle between the ecliptic plane and the plane containing the Earth, Sun, and observation direction (that is, the azimuth angle about the Earth-Sun axis). The value of  $I_0$  is zero when IRAS looks at the ecliptic plane in the direction opposite to the motion of the Earth around the Sun. The value increases clockwise around the Earth-Sun axis when facing the Sun, and opposite from the direction of the motion of the satellite in its polar orbit about the Earth. These angles are related to geocentric ecliptic coordinates by

$$\cos(\theta) = \cos(\beta)\cos(\lambda-\lambda_0)$$

$$\sin(I_0) = \sin(\beta)/\sin(\theta)$$

where  $\beta$  is ecliptic latitude,  $\lambda$  is ecliptic longitude, and  $\lambda_0$  is the longitude of the Sun. Figure 1 illustrates the IRAS native coordinate system of solar elongation  $\theta$  and observation inclination  $I_0$ . Inclination  $I_0$  is related to the IRAS clock angle  $\phi_0$  by

$$I_0 = 90 \text{ degrees} - \phi_0$$

where the clock angle  $\phi_0$  is measured in the plane perpendicular to the Sun line and clockwise as viewed from the Sun.

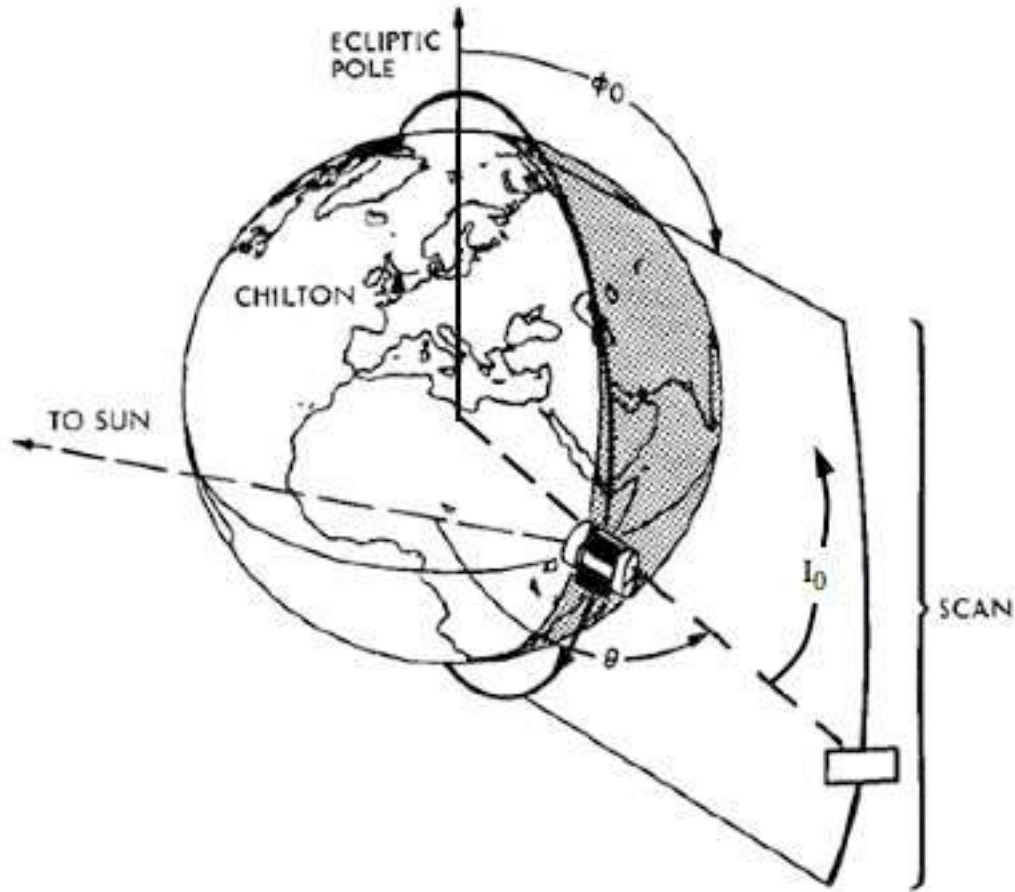


Figure 1. A solar elongation and clock angle system defines the geometry of a scan. The solar elongation angle  $\theta$  is the angle between the satellite-to-Sun line and the boresight. The IRAS clock angle  $\phi_0$  is measured in the plane perpendicular to the Sun line and clockwise as viewed from the Sun. Sometimes the inclination of the IRAS observation,  $I_0 = 90 \text{ degrees} - \phi_0$ , is used.  $I_0$  is the angle between the ecliptic plane and the plane containing the Earth, Sun, and observation direction (that is, the azimuth angle about the Earth-Sun axis). This graphic was copied from the IRAS Explanatory Supplement, available online at the IPAC website, <http://irsa.ipac.caltech.edu/IRASdocs/exp.sup/ch3/B.html>.

The images were constructed by referencing the radiance samples to the orbital position of the comet at the time of the sample. Thus the comet (by virtue of its orbital elements) is always at pixels 75 and 37. This is the map center reference and has mean elongation and inclination as given in the header. However, as in the header above the maximum radiance of the comet (COMETMAX) did not occur at 75,37 but at 77,37. The pixel size is 24 x 24 arcsec. Also note that in this image the maximum radiance (DATAMAX) does not occur at the comet (COMETMAX). This is a map of the radiance and includes background radiance, thus DATAMIN = 0 and the comet radiance is biased up by the background radiance.

Since the images are constructed from many survey scans at different times, the mean coordinates (RA, DEC, Elongation, Inclination) were listed for the comet at the mean Julian Date (MEAN JD). Scans that occurred at nearly the same heliocentric and geocentric distances were selected. The sSOP\_Band.log files and the survey\_scans\_used.tab contain much helpful data on this, and are self-explanatory. You will encounter the time variable UTCS. This is IRAS time. It may be converted to Julian date by

$$JD = 2445335.5d0 + (UTCS - 63072000.0d0) / 86400.0d0$$

The UTCS start and stop times for each image were converted to UTC Julian dates and Gregorian dates and included in the FITS headers.

Although the images are binned into 24" pixels, the actual resolution within the image is dependent on (among other things) the number of iterations. All iterations were ran until the variations of the flux within each pixel (that was actually scanned) had converged to within the photometric noise of that pixel. There was no direct measure of the spatial resolution achieved, however, Rice (1993) measured the mean dimensions of 13 bright IRAS stellar point sources as a function of the number of iterations. The Rice (1993) results in the following table:

Table 0. FWHM Cross-scan x In-scan (arcsec)				
MCM Iteration	12 $\mu$ m	25 $\mu$ m	60 $\mu$ m	100 $\mu$ m
01	256 x 64	270 x 67	301 x 121	403 x 282
05	79 x 34	72 x 36	123 x 63	182 x 134
10	51 x 28	48 x 28	86 x 50	131 x 103
20	37 x 23	35 x 23	62 x 41	98 x 80
Notes: 1. Uncertainties in the mean dimensions are less than 8%				
2. The geometric detector beam is ~ 300" cross-scan and ~ 45", 45", 90", and 180" at 12, 25, 60, and 100 $\mu$ m respectively along the in-scan direction.				
3. Little or no improvement of resolution was noted after 20 iterations.				

### Aperture Photometry

The data set that Russell Walker delivered included aperture photometry files. However, the original photometry files will be replaced by photometry data being derived by and published for the Deep Impact Mission. Neither of these photometry data is included in this archive; the new photometry data will be archived in the future. This Aperture Photometry section remains in the document as a record of Russell Walker's photometry work.

## Aperture Photometry - File Designations and Content

IRAS Survey Scans are identified by a satellite operations plan (SOP) number. The images and photometry tables are identified by a “mean” SOP number, since several scans are used to make an image. The IRAS observations were made in four spectral bands centered nominally at 12 $\mu$ m, 25 $\mu$ m, 60 $\mu$ m, and 100 $\mu$ m. Photometry files are supplied for the final iteration (nn) determined by the convergence of the flux in all the pixels in the scanned path. Thus, the following file names were adopted for the Survey Scan photometry tables:

Radiance Photometry Files (20) – sSOP\_Band\_Iteration#\_radiance.tab  
Noise Photometry Files (20) – sSOP\_Band\_Iteration#\_noise.tab

The numbers in parenthesis above are the number of files that PDS-SBN received. Values for Band are 12 $\mu$ m, 25 $\mu$ m, 60 $\mu$ m, and 100 $\mu$ m. Iteration value is for the iteration final iteration (15 through 40).

## Aperture Photometry - Methodology

The radiance (and noise) photometry files are the result of summing the radiance (and variance) from all the pixels that are within a selected distance from the pixel of maximum comet radiance. There are three columns in the files. The first is the distance (radius) that includes the pixels summed. Zero is the central pixel, etc. The second column is the summed radiance (or noise) in units of Watts cm<sup>-2</sup>. The third column is the number of pixels actually included in the sum. Most of the coma flux should be contained within a few pixels radius. There is 0.846125 x 10<sup>-8</sup> steradian per 15” square pixel or 2.166080 x 10<sup>-8</sup> steradian per 24” square pixel.

The original photometry files delivered to PDS-SBN during December 2000 for the Survey Scan Images used the image median to estimate the background and subtract that from the image prior to photometry. This is usually a reasonable thing to do for stars, etc. However, for the comet, the dust tail may be a significant source of background (or foreground) for estimates of the coma flux (see Figure 2a). In the case of a point source in a uniform background one expects the aperture photometry curve to rise to an asymptotic value if the background has been properly subtracted (Figure 2b). R. Walker modified his photometry program to iterate the background radiance until the profile tends toward asymptotic at radii greater than 30 pixels from the maximum comet radiance. He chose to call this “coma aperture photometry” and the value of the asymptote an estimate of the total coma flux. The difference between of the original and revised methods for estimating the background is illustrated in Figures 1a and 1b. The revised fluxes for the survey scan data, generated by the “coma aperture photometry” process, and are presented in Table 1.

Photometry for the survey scan images was redone by R. Walker using the new software and radiance survey “coma” photometry files were delivered to PDS-SBN in February 2001 (data/survey/phot/).

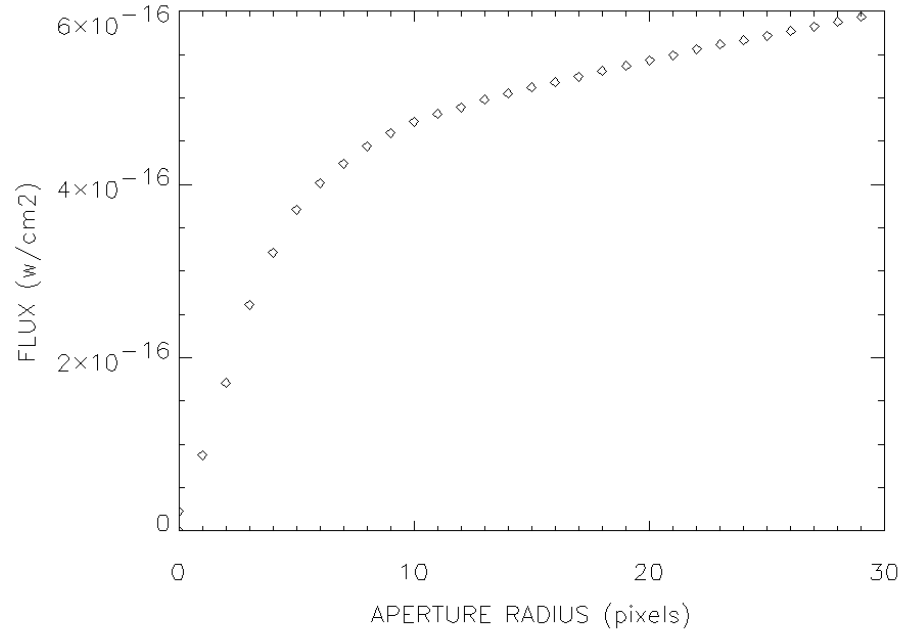


Figure 2a. Aperture photometry of the 12  $\mu\text{m}$  survey radiance image #339 with median background subtraction as delivered on December 29, 2000.

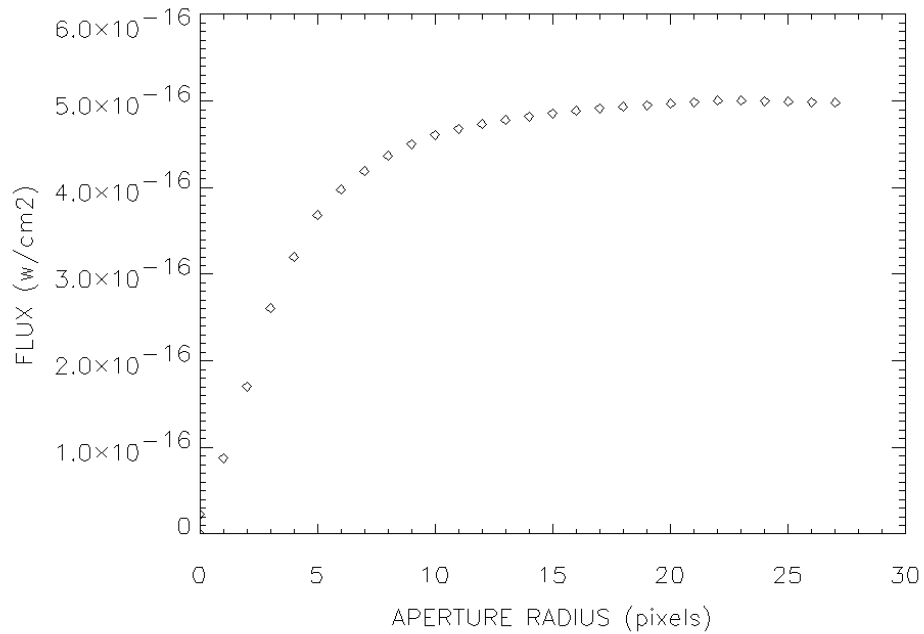


Figure 2b. Aperture photometry of the 12  $\mu\text{m}$  survey radiance image #339 with iterative background subtraction (coma photometry).

Table 1. Results of “Coma” Aperture Photometry on the Survey Observations						
SOP	OBS	RHO (AU)	DELTA (AU)	BAND ( $\mu\text{m}$ )	FLUX ( $\text{w cm}^{-2}$ )	REMARKS
339		1.491	0.976	12	$4.99 \times 10^{-16}$	
				25	$3.97 \times 10^{-16}$	
				60	$7.03 \times 10^{-17}$	
				100	$7.16 \times 10^{-18}$	Noise/Background Structure
368		1.503	1.064	12	$4.14 \times 10^{-16}$	
				25	$3.55 \times 10^{-16}$	
				60	$6.63 \times 10^{-17}$	
				100	$8.79 \times 10^{-18}$	Noise/Background Structure
389		1.521	1.138	12	$3.65 \times 10^{-16}$	
				25	$2.86 \times 10^{-16}$	
				60	$6.05 \times 10^{-17}$	
				100	$6.90 \times 10^{-18}$	Noise/Background Structure
421		1.561	1.265	12	$2.96 \times 10^{-16}$	
				25	$2.69 \times 10^{-16}$	
				60	$(6 \times 10^{-17})$	Background Structure
				100	?	Noise/Background Structure
493		1.695	1.624	12	$(1.8 \times 10^{-16})$	Crowded Field
				25	$(1.3 \times 10^{-16})$	“
				60	$>5.3 \times 10^{-17}$	“
				100	?	Noise/Background Structure

### Comments on Colors and Flux Measures

One can convert the in-band radiance ( $\text{w cm}^{-2} \text{sr}^{-1}$ ) to flux density units ( $\text{Jy sr}^{-1}$ ) by dividing the in-band radiance by  $(13.48, 5.16, 2.58, \text{ and } 1.00) \times 10^{-18}$  for the 12, 25, 60, and  $100\mu\text{m}$  bands respectively. This must then be corrected for the spectrum of the source, for example: for a blackbody at 250K the flux densities must be divided by 0.87,

1.11, 1.19, and 1.07 for the 12, 25, 60, and 100 $\mu$ m bands respectively. It is recommended that model spectral radiances be integrated over the IRAS spectral response and compared to the observed in-band radiances rather than converting the observations to flux densities.

Colors (flux ratios) are a more complicated problem. Even after running the MCM high-resolution process the spectral bands have different resolutions. Ratios made from the 12 $\mu$ m and 25 $\mu$ m bands will have meaning since these two bands have virtually the same resolution at all iteration steps. However, if one wants to compare radiance ratios, say,  $R(12\mu\text{m})/R(60\mu\text{m})$ ,  $R(25\mu\text{m})/R(60\mu\text{m})$ , etc. he will not obtain the desired result due to the different beam sizes involved. There are two sophisticated ways to approach this problem: 1) *Cross-band simulation* wherein a new set of images is made by scanning the high-res images with a simulation of the IRAS focal plane, running MCM on these new images to produce images that have the same resolution and can then be ratioed. 2) *Prior-knowledge* technique wherein say the 60 $\mu$ m high-res image is used as the starting point for constructing a 100 $\mu$ m image and vice versa. This technique results in an image of higher resolution than the cross-band technique. Both of these methods are described by Fowler and Aumann (1994).

A simple approach would use the beam-size information in the above table to estimate the two-dimensional gaussian beam profile necessary to convolve with the higher resolution image to produce an image at the resolution of the lower resolution image. These can then be ratioed for comparison to calculated spectral ratios. For example: one wishes to ratio a 20 iteration 12 $\mu$ m image with a 10 iteration 60 $\mu$ m image; the FWHM of the gaussian kernel would be 1) cross-scan:  $\sqrt{86^2 - 37^2} = 77.6$  and 2) in-scan:  $\sqrt{50^2 - 23^2} = 44.4$ . The 12 $\mu$ m map is then convolved with the 77.6 x 44.4 kernel and the two maps ratioed. Values for other numbers of iterations and band combinations can be interpolated in the table. The assumption that the output PSF of MCM is gaussian is not really a bad one.

In addition, the noise images are good measures of the relative noise from one part of an image to another. They are poor estimates of the absolute noise level. The photometric noise map indicates the internal photometric error of the detector samples resulting from the averaging of overlapping samples. It does not include absolute errors such as calibration errors. This applies to both the survey and additional observations (AO) data. Beichman, et al (1988) estimates that the absolute errors in the IRAS absolute calibration are 2%, 5%, 5%, and 10% at 12 $\mu$ m, 25 $\mu$ m, 60  $\mu$ m, and 100 $\mu$ m respectively due to uncertainty in the models used. These numbers should be RSSd with 3% uncertainty in the standard stars used and 4% uncertainty for spectral bandpass errors. I have removed some systematic errors by re-calibrating IRAS in accordance with Cohen, et al (1992). Thus an estimate of the uncertainties of the radiance data can be had by combining the above absolute errors with the noise map values in the root sum squared sense.

### Some Interesting Plots

Figure 3 is a plot of the “coma” fluxes from survey scans in Table 1 and additional observations (AO) in Table 2. “Coma” fluxes from the tables are divided by the pre-perihelion “coma” flux (s287 o13). Curvature in these plots is an indication of spectral variations at differing heliocentric distances. The heliocentric distances are labeled on the plot. One expects the spectrum to change due to variations in grain temperature, size distribution, and possibly composition.

Table 2. Results of “Coma” Aperture Photometry on the AO Observations						
SOP	OBS	RHO	DELTA	BAND	FLUX (w cm <sup>-2</sup> )	REMARKS
287	13	1.507	0.853	12	5.89 x 10 <sup>-16</sup>	
				25	4.07 x 10 <sup>-16</sup>	
				60	6.78 x 10 <sup>-17</sup>	
				100	8.98 x 10 <sup>-18</sup>	
407	12	1.541	1.204	12	3.63 x 10 <sup>-16</sup>	
				25	2.60 x 10 <sup>-16</sup>	
				60	4.02 x 10 <sup>-17</sup>	
				100	4.88 x 10 <sup>-18</sup>	Noise/Structure
407	43	1.541	1.206	12	3.56 x 10 <sup>-16</sup>	
				25	2.67 x 10 <sup>-16</sup>	
				60	4.53 x 10 <sup>-17</sup>	
				100	4.91 x 10 <sup>-18</sup>	Noise/Structure
509	40	1.735	1.725	12	?	Source Confusion
				25	?	“
				60	?	“
				100	?	“
510	22	1.737	1.730	12	?	Source Confusion
				25	?	“
				60	?	“
				100	?	“

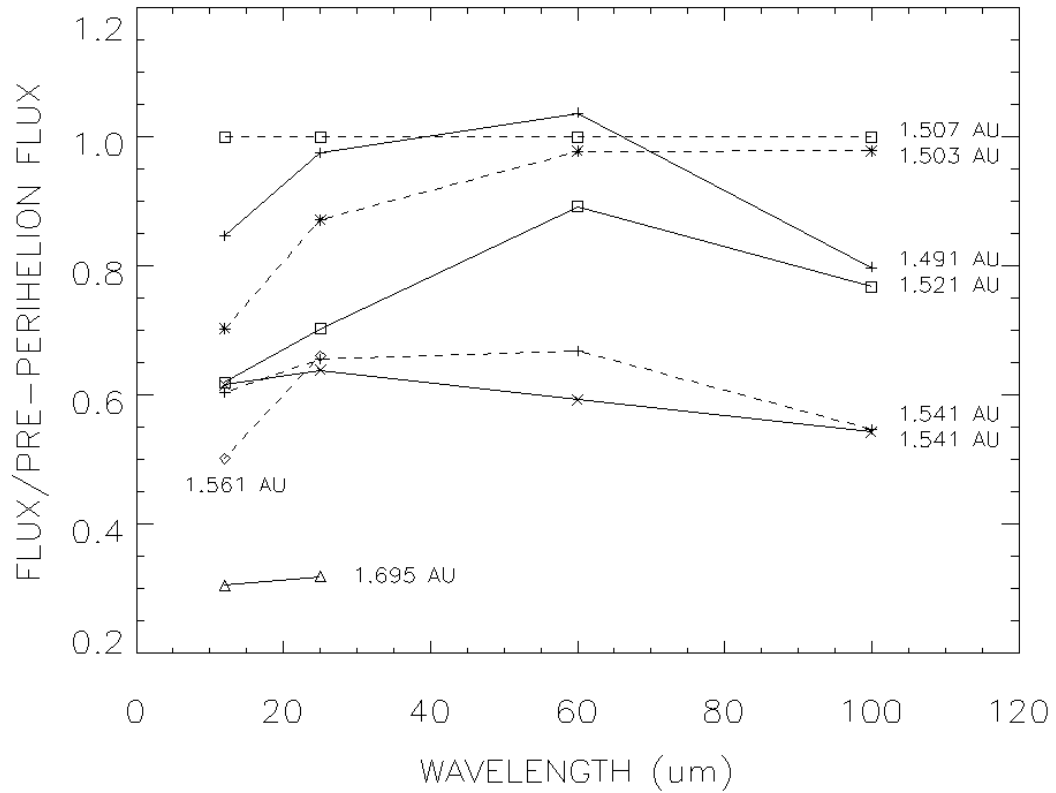


Figure 3. Tempel 1 spectrum relative to its pre-perihelion spectrum at 1.507 AU.

Figure 4 is a plot of the relative “activity” of Tempel 1 as a function of heliocentric distance. The “activity” is defined as  $\Delta^2 \times \text{Flux}(\Delta)$ , where  $\Delta$  is the geocentric distance of the comet. This quantity is a measure of the dust production rate, or perhaps more properly, the resident time of dust within the beam. These data are normalized to the “activity” of the pre-perihelion observation. The heliocentric distances are labeled.

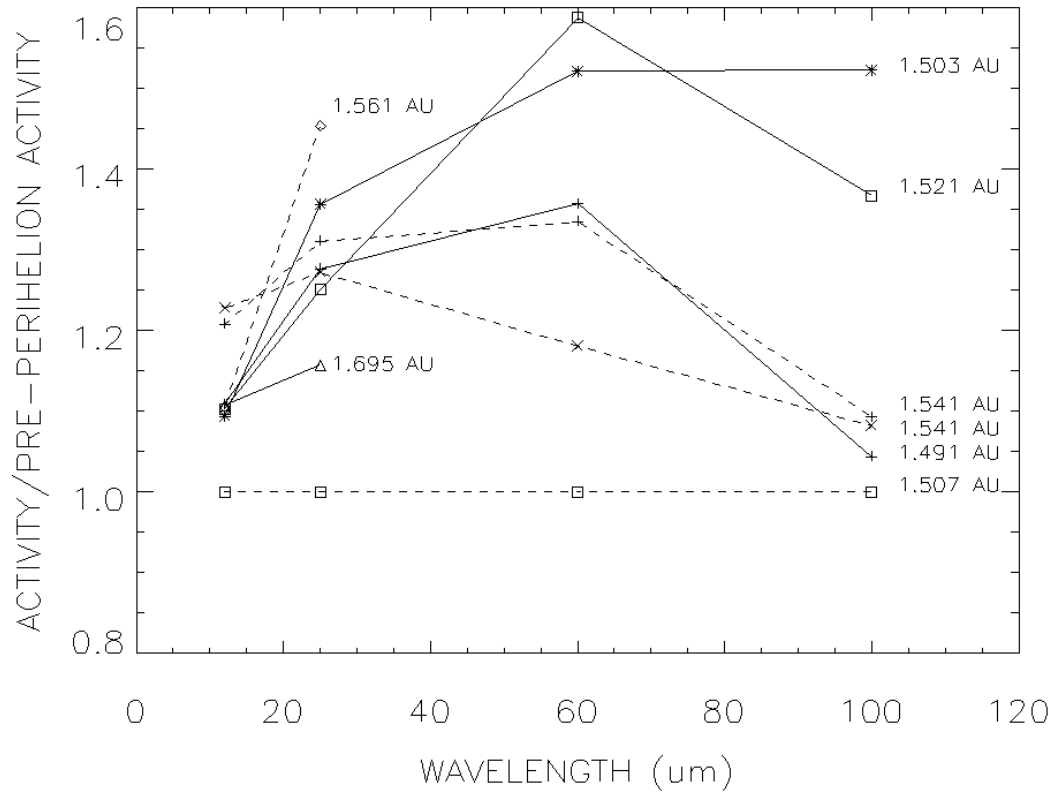


Figure 4. Activity of Tempel 1.

Table 3. Survey Scans Used

Scans used to create the survey images:

MEAN SOP	SOP	OBS	UTCS (sec)	JD (days)	RA (hour)	DEC (deg)	RHO (AU)	DELTA (AU)	PHASE (deg)	ELONGATION (deg)	UTCS(start) (sec)	UTCS(end) (sec)
339	338	27	79844009.36	2445529.62	13.699	-11.152	1.492	.975	42.562	96.497	79843985.36	79844033.36
	339	3	79850184.32	2445529.69	13.701	-11.181	1.492	.975	42.564	96.974	79850160.32	79850208.32
	339	9	79856375.02	2445529.76	13.704	-11.209	1.492	.976	42.565	96.951	79856351.02	79856399.02
	339	19	79862542.19	2445529.83	13.706	-11.238	1.492	.976	42.567	96.928	79862518.19	79862566.19
	339	27	79868737.28	2445529.91	13.709	-11.266	1.492	.977	42.569	97.405	79868713.28	79868761.28
	339	36	79874904.18	2445529.98	13.712	-11.295	1.492	.977	42.570	97.382	79874880.18	79874928.18
	339	45	79881083.18	2445530.05	13.714	-11.323	1.492	.977	42.572	97.359	79881059.18	79881107.18
368	367	27	81087172.42	2445544.01	14.252	-16.695	1.503	1.061	42.436	92.237	81087148.42	81087196.42
	367	30	81093338.99	2445544.08	14.255	-16.721	1.503	1.061	42.433	92.218	81093314.99	81093362.99
	367	33	81099504.81	2445544.15	14.258	-16.747	1.503	1.062	42.430	92.698	81099480.81	81099528.81
	368	19	81130987.98	2445544.52	14.273	-16.881	1.504	1.064	42.416	92.599	81130963.98	81131011.98
	368	27	81136593.44	2445544.58	14.276	-16.905	1.504	1.065	42.413	92.580	81136569.44	81136617.44
	368	26	81142774.31	2445544.65	14.279	-16.931	1.504	1.065	42.410	92.561	81142750.31	81142798.31
	369	2	81148963.75	2445544.72	14.282	-16.957	1.504	1.066	42.407	93.041	81148939.75	81148987.75
	369	8	81155144.91	2445544.80	14.285	-16.984	1.504	1.066	42.405	93.022	81155120.91	81155168.91
389	389	8	82021150.24	2445554.82	14.717	-20.491	1.521	1.136	41.819	89.381	82021126.24	82021174.24
	389	14	82027343.81	2445554.89	14.720	-20.514	1.521	1.136	41.813	89.363	82027319.81	82027367.81
	389	19	82033537.15	2445554.96	14.723	-20.538	1.521	1.137	41.808	89.345	82033513.15	82033561.15
	389	26	82039730.88	2445555.03	14.727	-20.562	1.521	1.137	41.803	89.826	82039706.88	82039754.88
	389	31	82046201.37	2445555.11	14.730	-20.587	1.521	1.138	41.797	89.808	82046177.37	82046225.37
	390	34	82089207.50	2445555.61	14.752	-20.751	1.522	1.141	41.759	89.680	82089183.50	82089231.50
	391	2	82095390.09	2445555.68	14.755	-20.775	1.523	1.142	41.753	90.162	82095366.09	82095414.09
	391	7	82101574.27	2445555.75	14.759	-20.798	1.523	1.142	41.747	90.144	82101550.27	82101598.27
	391	13	82107749.53	2445555.82	14.762	-20.822	1.523	1.143	41.742	90.626	82107725.53	82107773.53
421	421	10	83399973.15	2445570.78	15.468	-25.267	1.560	1.263	40.269	85.403	83399949.15	83399997.15
	421	16	83406167.56	2445570.85	15.471	-25.285	1.560	1.263	40.261	85.385	83406143.56	83406191.56
	421	23	83412361.80	2445570.92	15.475	-25.304	1.561	1.264	40.252	85.867	83412337.80	83412385.80
	421	30	83418556.84	2445570.99	15.478	-25.323	1.561	1.265	40.244	85.849	83418532.84	83418580.84
	421	35	83424751.15	2445571.06	15.482	-25.342	1.561	1.265	40.236	85.832	83424727.15	83424775.15
	421	41	83431383.14	2445571.14	15.486	-25.362	1.561	1.266	40.227	86.313	83431359.14	83431407.14
	422	29	83468042.03	2445571.57	15.506	-25.472	1.562	1.270	40.177	86.208	83468018.03	83468066.03
	422	34	83474235.73	2445571.64	15.510	-25.491	1.563	1.270	40.168	86.190	83474211.73	83474259.73
493	491	31	86442399.77	2445605.99	17.283	-31.342	1.693	1.618	35.138	76.062	86442375.77	86442423.77
	491	38	86448584.78	2445606.06	17.287	-31.348	1.694	1.618	35.126	76.541	86448560.78	86448608.78
	492	41	86491978.73	2445606.56	17.313	-31.388	1.696	1.624	35.042	75.893	86491954.73	86492002.73
	492	49	86498048.00	2445606.63	17.317	-31.393	1.696	1.625	35.030	76.373	86498024.00	86498072.00
	493	12	86510412.90	2445606.78	17.324	-31.404	1.697	1.627	35.006	76.330	86510388.90	86510436.90
	493	18	86516596.90	2445606.85	17.328	-31.410	1.697	1.628	34.994	76.309	86516572.90	86516620.90
	493	25	86522780.71	2445606.92	17.332	-31.415	1.697	1.628	34.982	76.788	86522756.71	86522804.71

NOTES:

1. UTCS and JD in columns 4 and 5 are the times that the IRAS boresite crossed the comet.
2. RA and DEC (B1950) are the coordinates of the comet at the time of crossing.
3. RHO and DELTA are the heliocentric and geocentric distance of the comet at the time of crossing.
4. ELONGATION is the solar elongation of the comet at the time of crossing.
5. UTCS(begin) and UTCS(end) are the beginning and ending times of the scan.

## References

- Aumann, H.H., Fowler, J.W., Melnyk, M., 1990, "A Maximum Correlation Method for Image Construction of IRAS Data", *Astron. J.* 99, 1674-1681.
- Beichman, et al, 1988, 'IRAS Catalogs, Vol 1. Explanatory Supplement'.
- Cohen, M., Walker, R.G., Barlow, M.J., Deacon, J.R., 1992, "Spectral Irradiance Calibration in the Infrared. I. Ground-based and IRAS Broadband Calibrations", *Astron. J.* vol. 104, no. 4, pp1650-1657.
- Fowler, J.W. and Aumann, H.H., 1994, "Science with High Spatial Resolution Far-Infrared Data, Proceedings of a Workshop Held 14-16 June 1993", JPL Publication 94-5, (S.Terebey and J. Mazzarella, Eds.).
- Melnyk, M., 1990, "Technical Reference to the Full Resolution Survey Coadd (FRESCO)", IPAC User's Guide, Ed.4, Part VR, California Institute of Technology.
- Melnyk, M. and Rice, W, 1991, "High Resolution Processing", IPAC User's Guide, Ed.4, Part VI, California Institute of Technology.
- Moshir, M., 1986, "Accessing Detector Response Function Data", IPAC, Interoffice Memo, 240-86-103 (1).
- Rice, W., 1993, "An Atlas of High Resolution IRAS Maps of Nearby Galaxies", *Astron. J.* Vol 105, pp 67-96.